Activated-carbon/TiO2 composites preparation: An original grafting by milling approach for solar water treatment applications

E Ribeiro, Gael Plantard, F Teyssandier, F Maury, N Sadiki, D Chaumont, V Goetz

Journal Pre-proof

Activated-carbon/TiO_2 composites preparation: An original grafting by milling approach for solar water treatment applications

E. Ribeiro (Investigation) (Formal analysis) (Visualization) (Writing - original draft), G. Plantard (Conceptualization) (Methodology) (Supervision), F. Teyssandier (Methodology) (Supervision) (Validation) (Writing - review and editing), F. Maury (Conceptualization) (Validation) (Writing - review and editing), N. Sadiki (Resources) (Formal analysis), D. Chaumont (Investigation) (Resources), V. Goetz (Conceptualization) (Methodology) (Supervision)

PII: S2213-3437(20)30463-2

DOI: https://doi.org/10.1016/j.jece.2020.104115

Reference: JECE 104115

To appear in: *Journal of Environmental Chemical Engineering*

Received Date: 2 March 2020

Revised Date: 25 April 2020

Accepted Date: 25 May 2020

Please cite this article as: { doi: https://doi.org/

Activated-Carbon/TiO_2 composites preparation: An original grafting by milling approach for solar water treatment applications

E. Ribeiro[(*,1,2)], G. Plantard[(1,2)], F. Teyssandier[(1)], F. Maury[(3)], N. Sadiki[(1)], D. Chaumont[(4)], and V. Goetz[(1)]

[(1)] PROMES CNRS, UPR 8521, Rambla de la thermodynamique 66100 Perpignan, France.

[(2)] University of Perpignan Via Domitia, 52 Paul Alduy 66100 Perpignan, France.

[(3)] CIRIMAT, ENSIACET-4 allée E. Monso, 31030 Toulouse, France.

[(4)] Laboratoire interdisciplinaire Carnot de Bourgogne, UMR 6303 CNRS-Université de Bourgogne, 9 Avenue Alain Savary, BP 47870, F-21078 Dijon Cedex, France.

* Corresponding author. Tel.: +33602311658.

E-mail address: enrique.ribeiro@promes.cnrs.fr

Graphical abstract

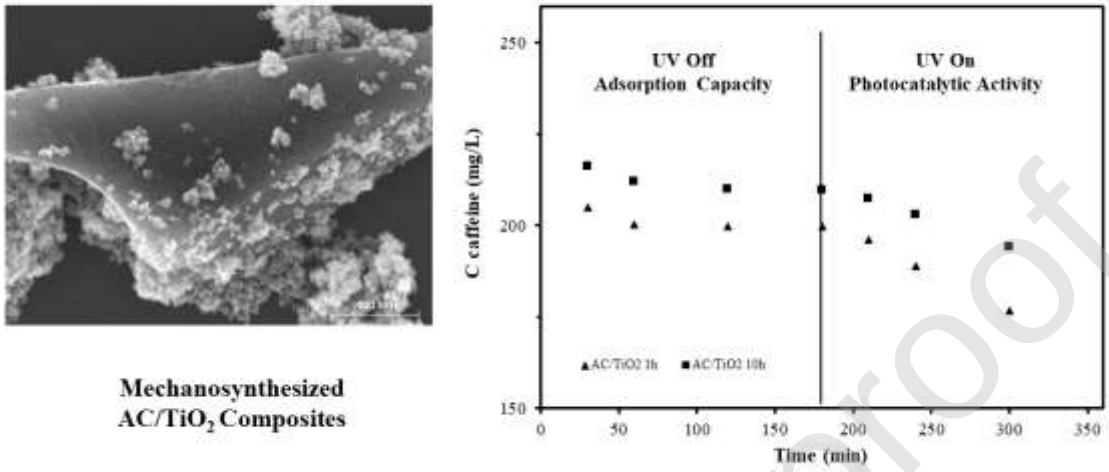

Highlights

- AC/TiO_2 Composites have been synthesized by a new approach
- Synthesis parameters study led to a control of the composite powder particles size, distribution and homogeneity
- Adsorbent and photocatalytic properties have been quantified showing multifunctional behavior of AC/TiO_2

Abstract

The aim of this work was to highlight feasibility of a new approach to synthesize Activated-Carbon (AC)/TiO_2 composite materials. The main interest of these materials is for pollutants removal applications thanks to their multi-functionality. AC/TiO_2 composites were prepared by one-step mechanosynthesis route. Morphological and structural properties were investigated through SEM, EDS, XRD, and BET techniques. It was found that the preparation process leads to the formation of an aggregate shape homogenously composed AC/TiO_2 powder with a narrow particles size distribution, which mean diameter was 3.75 µm. Initial component structural properties were found to be strongly affected by the process, resulting in significant changes of TiO_2 crystallinity and AC microtexture. The introduction of 5 min pauses during the process was enough to totally preserve TiO_2 phases, crystallinity, and AC microporous network. Composites multi-functional properties were investigated using batch adsorption and photodegradation experiments. Adsorption studies revealed that AC/TiO_2 aggregates exhibit good adsorption capacity with caffeine and a maximum adsorbed amount of 353 $mg.g^{-1}$. Photocatalytic experiments highlighted that AC/TiO_2 presents a photo-oxidation ability. Photodegradation apparent kinetic rate fitted with a first-order law gave a value of 1.04×10^{-5} s^{-1} for the composite and ten times higher for pure TiO_2. These results allowed to conclude that mechanosynthesis is an effective route to produce bi-functional AC/TiO_2 composites with efficient adsorption capacity for water treatment applications. It also suggests the need of further radiative transfer studies to understand light scattering and absorption inside these materials, which could lead to some improvement of these promising materials.

Keywords: *mechanosynthesis, composites, photocatalysis, adsorption, water treatment.*

1- Introduction

Last decades, the growing number of persistent pollutants in water became an issue threatening human health and environment. To break this deadlock, technologies such as adsorption [1-4], and advanced oxidation processes [5-9] allowed the removal of a wide range of target pollutants, respectively by separation or degradation processes. Removing pollutants by adsorption has appeared to be an effective simple technique, but there is still an economic issue as both the production of the adsorbent and its regeneration induce high energy consumption. On the other hand, because advanced oxidation processes (AOP) can generate radicals that are hugely effective at degrading recalcitrant pollutants, they have promoted more than a decade of intensive research to cope with the challenging task of cleaning water and air. Among them, Microwave-induced catalytic oxidation (MICO) and Photocatalytic AOPs have emerged as leading candidates for these applications: the first process, because of its low cost, high and fast degradation efficiency [5], and the second one, because of its good degradation efficiency and the attractiveness of using an environmentally-friendly solar-powered process [6-9]. There are two types of photocatalysis process, named 'homogeneous' and 'heterogeneous', where homogeneous refers to a process involving only one phase, *i.e.* both the catalyst and reactant medium are present in a liquid phase, and heterogeneous refers to a process involving two or more phases: typically a solid photocatalyst with a liquid and/or gas medium.

The electronic structure of semiconductor photocatalysts reveals a bandgap between the conduction band (CB) and the valence band (VB). When the activation energy is reached, e^-/h^+ pairs are dissociated, triggering other chemical reactions. When these semiconductor materials are used in aqueous media, the free h^+ react with water molecules and the free e^- react with oxygen dissolved in water, leading to the formation of very reactive radicals ($OH^{\bullet}$, $O^{2-\bullet}$). There are many heterogeneous semiconductor photocatalysts, among them TiO_2 has attracted most

research due to its low toxicity, chemical stability in water, and availability [10,11]. However, despite these properties, TiO_2 requires UV photo-excitation because of the 3.23 eV bandgap required to separate its VB electrons from the holes.

In the solar radiations, such an energy level represents only 5% of the spectrum [7], leading to a maximum potential available flux density of about 50 $W.m^{-2}$. Another explanation for the low photocatalytic activity of TiO_2 under solar radiation is the fast recombination time of photo-generated e^- and h^+ charges of about 10^{-9} s, as compared to the chemical reaction time between TiO_2 and adsorbed pollutants, which lies in the range 10^{-8}–10^{-3} s [12,13]. Eventually, it is well known that the sun is an intermittent source of radiation at different timescales: weather conditions evolving within a day, as well as day/night cycles and seasonal cycles. One strategy to overcome these intermittences and to improve photocatalytic activity is to optimize the use of solar radiation by coupling the TiO_2 photocatalyst with adsorbent materials, allowing pollutants to be adsorbed close to photocatalytic sites, thereby enhancing the oxidation process [14-16].

Activated carbon (AC) is a popular adsorbent choice for water treatment applications due to its non-selectivity and high porosity that confers a great potential for removing a wide range of water pollutants [17-20]. Moreover, adsorption on AC is mainly driven by physical adsorption, which makes it reversible and amenable to adsorption/desorption cycles [17,21,22]. This behavior raised interest in combining different forms of carbon with TiO_2, and it was reported that the two materials exhibited a synergistic effect enabling (i) a better photocatalytic efficiency [23-26] through the availability of high-quality adsorptive-active sites and a minimization of electron/hole recombination and bandgap tuning, and (ii) a partial regeneration of previously saturated AC driven by the photocatalytic process [27-30].

There has consequently been a lot of papers published on pairing AC/TiO_2 in a wide range of synthesis processes, the most popular being sol-gel [31-33] as the process is simple to implement and control. Strong chemical bonding and well-dispersed TiO_2 particles at the surface of the AC material surface have been observed when using high purity nanosized TiO_2 particles. However, the process is slow and requires long synthesis times, high calcination temperatures, and expensive reagents [34,35]. Chemical vapor deposition is another well-studied process for AC/TiO_2 composite synthesis [13,31,36]. It enables in-process reduction and activation of the catalyst and can be driven continuously, thus facilitating industrial-scale applications. However, the technique requires high temperature and low-pressure conditions and the supply of high-purity inert gas, while many by-product gases are created throughout along the synthesis process [37]. There are host of other processes available, each bringing their own advantages, but they tend to come with one or more disadvantages too such as being either expensive on chemicals, time-consuming, and/or hard to implement [38]. Furthermore, the studies dealing with AC/TiO_2 composite materials synthesized using all these methods point out the lack of interactions between AC and TiO_2 [31]. The challenge now is to develop a simple method that overcomes these issues using an industrially scalable yet environmentally-friendly process.

Several solid-state synthesis methods have recently attracted increasing interest because they are cheap and environment-friendly. They furthermore require short synthesis times and can be either liquid-assisted or solvent-free [39,40]. One such technique is mechanosynthesis, which synthesizes materials using mechanical energy, and has been widely used for decades to produce ceramics [41], metal alloys [42], and organic materials [43]. Much of its success comes from the ability of this process to maintain the interesting properties of the combined materials. The method was first used to alloy ductile pairs of materials [44,45], but there have since been numerous reports of ductile-brittle associations, generally resulting in oxide dispersion of the

brittle material in the ductile matrix [45,46]. Reports on brittle-brittle associations are rare because it remains a real challenge to alloy two brittle materials, as their particles tend to fracture rather than flatten and weld [45,47]. For AC/TiO_2 composites at least one component is a brittle material and no studies related to their preparation by mechanosynthesis were found.

This paper explores the feasibility of grafting TiO_2 on AC by milling, using a mechanosynthesis process, to produce multi-functional composite materials. Both raw materials (AC and TiO_2) and a mixture including a specific AC/TiO_2 ratio were milled through the process for different times and following two different processing routes, *i.e.* continuous milling and intermittent milling. First, we investigated the influence of synthesis conditions on their morphological, textural, and structural properties. As the goal remains to reach double functionality for solar water treatment applications, we evaluated the functional properties of the composite materials via two serial tests: (i) adsorption measurements applied to all samples using an experimental batch set-up and (ii) photocatalytic experiments conducted under controlled UV irradiation.

2- Experimental

2.1- Starting materials and mechanosynthesis

Composite materials were synthesized starting from commercial TiO_2 and AC powders. Aeroperl® TiO_2 P-25 powder was chosen as photocatalytic material due to its high photodegradation capability and particle granulometry (*i.e.* micron-size aggregates with an average diameter of about 25 µm, composed of nanometric crystallites). The crystalline phase composition referred to the supplier is 80%$_w$ anatase and 20%$_w$ rutile. Commercial AC Picahydro SP23 (Pica, France) was obtained by physical activation of coconut shells through a

steam flux. It has an average particle size of about 10 µm and a specific surface area of around 1000 m^2/g. It is designed for the adsorption of high-concentration micro-pollutants like volatile organic compounds (VOC) and hydrocarbons from water.

In order to form AC/TiO_2 composites having strong connections between the two components, they were synthesized via well-established protocols. Samples were prepared using a Fritsch Pulverisette 6 (P6) planetary ball mill. Process parameters were optimized beforehand as follows. Zirconium oxide was chosen as bowl and milling balls (grinding media) material due to its high refractory properties and chemical inertia in the process conditions and also because of its hardness compared to ground materials. A small 45 mL grinding bowl was used to process these experiments. We used the smallest milling balls available (3 mm in diameter) to improve the control of the ball-to-powder mass ratio (10:1), which was chosen as the most common ratio when using small grinding balls [45]. In practice, a total powder mass of 10 g was introduced in the mill together with 100 g of 3 mm zirconium oxide balls. The mill was then closed before handling the running parameters. Process rotation speed was set at 400 rpm to maximize grinding speed and avoid reaching what is referred to in the literature as the upper speed limit [45]. Milling time was set between 1–10 h to investigate the impact of the processing time on the synthesized structures. Furthermore, two milling protocols were applied: (i) Continuous Milling (CM) for the selected time and (ii) Intermittent Milling (IM), with 5 min pauses after every 15 min of milling. This second protocol was selected to test its potential ability to at least partially preserve the structural properties of the milled materials [48]. The AC/TiO_2 powder mass ratio was 3:7. Four composite samples were synthesized to cover different milling times using the protocols described above. These composites were named 1h-CM-AC/TiO_2, 10h-CM-AC/TiO_2, 1h-IM-AC/TiO_2 and 10h-IM-AC/TiO_2 the first part of their name being the milling time and the second part being the milling protocol (Continuous or Intermittent milling). The powder mixture was sealed in the zirconia mill under ambient

atmospheric pressure and temperature conditions. To preserve structural properties and be used as reference component for comparing functional properties with the composites, a set of samples was prepared in the same way as described above using individually each component, TiO_2 and AC.

2.2- Characterization methods

A structural characterization investigation was conducted to check the preservation of some interesting properties such as the materials crystallinity, their microtexture, the powder particles shape and size distribution, and the AC/TiO_2 composite stability. Samples were analyzed by X-ray diffraction (XRD) at room temperature using a PANalytical XPert Pro powder diffractometer (Cu-Kα radiation at 40 kV and 40 mA, λ = 1.5418 Å). X-ray diffraction measurements were carried out over an angular range of 20 to 70°. The step size and the time per step were fixed at 0.01 and 20 s respectively. The X-ray diffraction spectra were recorded and studied using the PANalytical software. The contribution from Cu-$K\alpha_2$ X-ray was removed. The instrumental function was determined using a reference material (SRM 660, lanthanum hexaboride, LaB_6 polycrystalline sample) and can be expressed by a polynomial function. The crystalline phases were identified by comparison of the obtained spectra with available models of standard references (powder diffraction file PDF-4 and International Center for diffraction data). The software used for data analysis and for the Rietveld refinement was HighScore Plus from PANalytical PDF-4 databases from the ICDD and ICSD for HighScore Plus software were used to identify the phases. The porous microstructure of the raw and intermittent milled materials was investigated using Brunauer-Emmett-Teller (BET) analysis. Surface area and pore size distribution were determined by N_2 adsorption at 77 K and 10 h degassing at 200°C using a Micromeritic TriStar II 3020 analyzer. Scanning electron microscopy (SEM-FEG,

Hitachi S-4500) was used to investigate the morphology and homogeneity of the powder samples. Images were acquired with a secondary electron detector and a 5 kV electron beam, at a working distance of 5 mm, and a x50 000 magnification. The composition of powder particles was analyzed by Energy Dispersive Spectroscopy (EDS) using KEVEX Si(Li) Brüker analyzer.

2.3. adsorption and photodegradation procedures

For the multi-functional properties, adsorption and photodegradation experiments were conducted using magnetically-stirred beakers containing 100 mL of caffeine solutions prepared with ultrapure water (18 MΩ). Reagent Plus-grade caffeine powder (> 99.0% purity) from Sigma-Aldrich USA, was chosen as a target pollutant molecule as it is recalcitrant to photodegradation [49] and safer to handle than most bio-recalcitrants. Experiments were performed under a 40 W neon source radiating at 370 nm to activate the photocatalyst by exciting the bandgap energy value. The lamp was off for adsorption experiments and turned on for photodegradation measurements. The adsorption experiment protocol was significantly different from the one used for photocatalysis experiments:

Under adsorption experiments, each beaker was filled with the same quantity of AC material to make the adsorption experiments comparable, because TiO_2 has a negligible adsorption capacity [38]; this means 0.1 g of powder for AC samples and 0.3 g of composite powder for AC/TiO_2 samples to respect the 3:7 mass ratio.

The photodegradation protocol was divided into two phases, the first for measurements of adsorption and the second for the photocatalytic behavior:

(i) UV lamp off: this period allows caffeine adsorption to reach the adsorption equilibrium of the sample/caffeine pair from t = 0 to 180 min. In solutions containing high caffeine concentrations, the adsorbent can be saturated and so some caffeine molecules remain in the

liquid phase. Experiments were carried out with the two composite samples and with both unmilled and milled TiO_2 (10h-CM-TiO_2 and 10h-IM-TiO_2) by adding the solutions with the same amount of TiO_2 material, *i.e.* 0.2 g of powder for TiO_2 samples and 0.3 g of composite powder for AC/TiO_2 samples. We used a 2 g/L concentration amount of TiO_2, which corresponds to the optimal concentration for the Aeroperl TiO_2 to absorb all the radiation in our experimental conditions (light crossing 2 cm of suspension), as reported elsewhere [50]. We chose a different starting caffeine concentration for each sample, thus allowing the second phase of photodegradation to be initiated at an almost equivalent caffeine concentration in the liquid phase for all samples.

(ii) UV Lamp on: this is the period of photocatalytic degradation of caffeine from t = 180 to 360 min.

For both adsorption and photodegradation experiments, caffeine concentration over time was followed by ultra-high-performance Liquid Chromatography on an Ultimate 3000 system equipped with a UV-Vis detector and a Hypersil GOLD C18 column (100 mm x 2.1 mm; particle size: 5 µm). An isocratic elution mode with detection at $\lambda = 274$ nm was used with a 90:10 (v/v) water:acetonitrile mixture at a flowrate of 0.6 $mL.min^{-1}$ to separate analytes. Stabilization of the caffeine concentration indicates that the adsorption equilibrium is reached between liquid phase and solid phase. The experiments were stopped when a slope lower than 0.4 $mg.L^{-1}.h^{-1}$ was observed during two successive samplings within a 30 min interval. This criterion was defined in a previous work [51]. In our experimental conditions, it corresponds to a variation of the adsorbed quantity of caffeine q lower than 2 $mg.g^{-1}$ over a 5 h time-interval. Isotherms were constructed by plotting equilibrium data, *i.e.* caffeine adsorbed in mg/gram of carbon material ($mg.g^{-1}$) against equilibrium concentration of caffeine in the solution ($mg.L^{-1}$). The adsorption and photodegradation measurements were reproducible, as observed in our

previous works [27,51]. However, note that each adsorption and photodegradation experiments measurements were realized three times in order to ensure the repeatability of the test.

3- Results and discussion

3.1- Morphological and structural properties

As mechanosynthesis is a powerful technique affecting the morphological and structural properties of milled materials, we first studied unmixed raw-milled materials in order to determine the synthesis conditions that best preserved the properties of interest of each component. We thus led assessment on process impacts for sample morphology and structure. As the photocatalyst properties are highly dependent on the crystalline network [52], we investigated the crystallinity of TiO_2 over the course of milling. We studied the porous network of both unmixed raw materials, as AC adsorption capacity depends largely on the micro-texture of the material. Then, we coupled compositional and particle-size analysis to evaluate the homogeneity and repeatability of the composite powders.

3.1.1. Crystallinity analysis

Rietveld refinement of XRD patterns [53] was used to characterize the crystalline-phase proportions. The average size of crystallites was estimated from the highest diffraction peak intensity using the Scherrer equation (Eq. (1)) considering crystallite as spherical and isotropic:

$$G = \frac{0.9\,\lambda}{B\cos\theta} \quad (1)$$

where G is the mean crystallite size (nm), 0.9 is the Scherrer constant introduced in the equation when using half-height width, λ is X-ray wavelength, B is half-height width of the most intense diffraction peak (rad), and θ is Bragg diffraction angle (°).

Figure 1 shows the XRD patterns of Continuously-Milled (CM), Intermittently-Milled (IM) and unmilled TiO_2 samples. Starting from the raw non-milled material (sample a), the diffraction angles and relative intensities of the diffraction peaks are in good agreement with powder diffraction standards data corresponding to the two tetragonal structures of TiO_2 with different space groups ($I4_1/amd$ and $P4_2/mnm$) called anatase (JCPDS #84-1286) and rutile respectively (JCPDS #88-1175). The diffraction peaks at 2θ = 25.28°; 36.95°; 37.85°; 38.58°; 48.07°; 53.97°; 55.07°; 62.75°; 68.95°; 70.25° can be respectively indexed to the A(101), A(103), A(004), A(112), A(200), A(105), A(211), A(118), A(116) and A(220) crystal planes of anatase (A). Additional diffraction peaks were observed at 2θ = 27.43°; 36.06°; 41.42°; 44.27°; 54.29°; 56.82° and 64.28° which can be respectively indexed to the R(110), R(101), R(111), R(210), R(211), R(220) and R(310) crystal planes of rutile (R). From the relative intensity of the main peaks in the raw TiO_2 sample the phase composition reveals 85 wt% of anatase in satisfactory agreement with the 80 wt% given by the supplier (Table 1).

Comparing with the raw TiO_2 sample, the anatase content decreases from 85 to 16 wt% while rutile increases from 15 to 45 wt% (Table 1). Interestingly a broad and small peak appeared at 2θ = 31.54°, likely another one in the background around 63-68 in the 10h-CM-TiO_2 pattern (sample c). These peaks can be attributed to the formation of brookite as they match well with the standard diffraction data of this phase (JCPDS #65-2448). Indeed, the peak at 2θ = 31.54° can be indexed to the B(211) crystal plane of brookite (B), and the broad peak between 63° and 68° can be indexed to B(521), B(123) and B(611) crystal planes. This result clearly shows a structural change from anatase to rutile and to brookite induced by the milling process conditions and an amorphization of the powder sample. It is well-known that rutile is less photoactive than anatase. Thus, this crystalline variation of TiO_2 is not favorable.

The 10h-IM-TiO_2 pattern (sample b) shows only a minor phase transformation, which was further confirmed through Rietveld analysis on all 3 samples since anatase content

decreases only from 85 to 79 wt% and brookite was not observed (Table 1). However, the pattern shows a broadening of both the anatase and rutile peaks, which was attributed to an amorphization, as confirmed by calculating the average crystallite size via the Scherrer equation (Table 1). As grain size is a major parameter for the TiO_2 phase stability at a nanometer scale, the formation of a brookite phase can be attributed to energy intake through the process promoting the most stable phase in this range of crystallite size (according to [54,55] brookite is the most stable phase for grain sizes in the range 9 to 37 nm). TiO_2 phase transformations have been extensively studied theoretically [56] and experimentally [57]. The heat released during the milling process promotes the anatase-to-rutile transition (sample c). The introduction of periodic pauses throughout the process prevents such a transformation (sample b).

3.1.2. Porous network variation

Figure 2 shows nitrogen adsorption-desorption isotherms (a) and the corresponding pore-size distribution curves (b) of the raw TiO_2 and AC starting materials, as well as the samples 1h-IM-AC, 10h-IM-AC, 1h-IM-AC/TiO_2 and 10h-IM-AC/TiO_2. First, Figure 2a shows that all AC samples fit a type-I isotherm as defined by the IUPAC classification scheme [58]. It corresponds to a monolayer adsorption on the micropores of the material, whereas TiO_2 fits a type-V isotherm, suggesting the presence of a mesoporous structure with low adsorption capacity. Composite samples showed an isotherm attributable to type-IV due to the presence of a saturation plateau (at p/p^0 = 0.2–0.7 for the 1 h alternately-milled sample and p/p^0 = 0.2–0.45 for the 10 h alternately-milled sample) and a hysteresis loop whose shape can be correlated to specific pore morphologies [59]. The hysteresis loop shape of 1h-IM-AC/TiO_2 fits type H3, which is characteristic of aggregates of plate-like particles with slit-shaped pores, whereas the hysteresis loop shape of 10h-IM-AC/TiO_2 fits type H4 which is similar to type H3 type but with narrow slit-like pores. It can reasonably be assumed that the longer milling time is responsible for the pore narrowing.

BJH analysis was used to obtain pore size distribution curves (Figure 2b). BET surface, micropore surface and external surface were also computed and reported in Table 2. Figure 2b clearly illustrates that AC is mainly composed of micropores, which is consistent with the shape of its isotherms. Mean pore size was not calculated as the results would be made unreliable due to the use of the TriStar device which is not accurate enough for micropore size analysis (< 2 nm). As expected, TiO_2 developed a very poor pore network. Finally, AC/TiO_2 composites gave a pore-size distribution midway between AC and TiO_2, but with a bulk share of mesopores. Mean pore diameters were calculated to be 8 nm for 1h-IM-AC/TiO_2 sample and 6.4 nm for 10h-IM-AC/TiO_2 composite (Table 2).

Comparative analysis of all samples showed that unmilled AC samples exhibited the best adsorptive capacities, with saturation plateaus from 290 to 495 cm^3/g at standard temperature and pressure conditions (Figure 2.a.). Adsorbed amount at saturation plateau differed for each AC sample, but the overall pattern was that more milling led to lower adsorption capacities. Results reported in Table 2 give a good explanation of what happens to AC through milling: BET surface diminished from 1742 to 1022 m^2/g. Further investigation found that AC milling (from 0 to 10 h) primarily affected external surface area, which decreased from 975 to 403 m^2/g. The partial preservation of AC features through intermittent milling can be attributed to a less energetic process which induces a more modest decrease in micropore surface area than external surface since micropore area diminished by only 20% through milling whereas external surface area diminished by almost 60%. Adsorbed quantity on the TiO_2 reference sample did not exceed 50 cm^3/g from relative pressure 0 to 0.85. The low adsorption capacity of the catalyst is well known and can be explained by its low BET surface, reported as 57 m^2/g (Table 2). As expected, composite samples showed intermediate adsorption capacities with saturation plateaus of 100 cm^3/g and 150 cm^3/g for 10h-IM-AC/TiO_2 and 1h-IM-AC/TiO_2 samples, respectively. This difference is in good agreement with results reported in Table 2: the

10h-IM-AC/TiO_2 sample had a 23% lower BET surface than 1h-IM-AC/TiO_2 composite. Like for the AC samples, AC/TiO_2 composite samples did not lose micropore area between 1 h and 10 h, which is assumed to explain the partial preservation of adsorption capacity in these samples.

3.1.3. Powders composition and granulometry

SEM-FEG micrographs of Figure 3 recorded at the same magnification show the morphology of intermittently-milled and unmilled samples of individual and composite materials. Note that AC samples still presented an irregular faceted shape even after 10 h of milling. SEM TiO_2 images showed an aggregate shape composed of nano-sized particles after milling. Note that this aggregation phenomenon is induced by the preparation process, because the unmilled TiO_2 image shows less-compact aggregates. AC/TiO_2 composite samples presented both AC and TiO_2 shape characteristics that visually distinguished AC (dark grains) from TiO_2 (light nano-crystals) Interestingly the composites were made of micrometric AC particles (forming aggregates when they are sub-micrometric) covered by TiO_2 nano-particles scattered on the surface of AC grains or forming small aggregates (Figure 3).

We studied the homogeneity of the composite powders by granulometric analysis using a home-made image processing protocol. First, 0.1 g of powder sample was mixed with 10 mL of acetone and sonicated for 15 min to obtain a well-dispersed suspension and break up the agglomerates. Then a few drops of the suspension were deposited on a flat silica substrate and left to air-dry for 1 min, thus dispersing composite particles on the substrate ready for imaging. Granulometric analysis was performed using the open source image processing program ImageJ on SEM micrographs acquired in high-resolution mode with an extraction voltage of 5 kV using a probe set at 5 mm distance. We computed volume density in relation to particle diameter as

follows: (i) particles on images were considered spherical, and their equivalent diameters were thus calculated from the surface area of each element; (ii) for each sample, around 100 images were taken depending on the particle number density of each image, aiming to reach at least 1000 particles for a representative granulometric analysis.

We cross-checked the efficiency of this home-made method on a simple raw TiO_2 powder run through a Mastersizer 3000 device via a normalized Dynamic Light Scattering (DLS) method using Mie theory. According to this theory, the use of DLS is restricted to well-defined particle shapes (generally spheres). In addition, optical properties are hard to define for composite particles, and misdefinitions add significant bias in this granulometric analysis method. These considerations prompted us to use another granulometric analysis method for the composite powders. The cross-checked powder analysis (Figure 4) allowed us to validate our home-made granulometric analysis method. Although clearly not as smooth as with the DLS method, the granulometric distribution curve given by our image processing method proved to be (i) sufficiently representative based on the good agreement between the two methods, and (ii) well adapted for the purpose of analyzing composite powders.

Figure 5 shows the composite granulometries for different milling times. The sample 1h-IM-AC/TiO_2 (A) resulted in a broad granulometric distribution whereas 2h-IM-AC/TiO_2 (B) gave a narrower granulometric distribution with significantly smaller particle sizes. After 5 h (C) of intermittent milling (5h-IM-AC/TiO_2), granulometric distribution looks like a clean gaussian function. This distribution narrowing can be attributed to both fracture of largest particles and welding of the smallest ones. After 10 h of intermittent milling (D), powder granulometry (10h-IM-AC/TiO_2) tends to center at 3.75 ± 0.25 µm with the narrowest distribution of all samples, and this trend was confirmed by results for the 20h-IM-AC/TiO_2 sample (E).

Average particle size, which was calculated from the granulometric analysis, varied from 20 ± 0.25 µm for unmilled samples down to 2.75 ± 0.25 µm for 20h-IM-AC/TiO_2 sample. Note that average particles size rapidly stabilized, as a 2 h milling time was enough to reduce the value to almost 4 µm. This trend is representative of what is generally observed over the course of mechanical alloying after a certain amount of time [45].

The chemical composition of powder particles was determined by EDS analyses coupled with SEM observations. The goal was not to provide a precise quantitative analysis but rather to assess the homogeneity of the ball-milled powder, as carbon is hard to quantify by EDS in our device configuration. We performed 10 analyses at different points of the sample and then recorded and reported the mean composition values in Table 3 with standard deviations. These results corroborated that the composite powders were homogeneously composed of about 30%$_w$ AC for the two samples, which is in good agreement with the initial mass ratio AC:TiO_2 = 3:7. There was lower standard deviation for the 10h-IM-AC/TiO_2 sample, which led us to assume that milling time increases powder homogeneity.

3.1.4. composites stability

The stability of AC/TiO_2 powders was checked by SEM observation of the composite morphology after undergoing the solicitation effects of two different environment i.e. (i) mechanical vibrations induced by sonication at 40 kHz in a bath sonicator for 30 min, which is expected to break agglomerates and low-cohesion aggregates and (ii) UV radiation exposition for 2 h under the lamp used for photocatalytic degradation experiments, which can affect the material by photocatalytic-induced reactions. 0.1 g of 1h-IM-AC/TiO_2 and 10h-IM-AC/TiO_2 powders were introduced in two beakers filled with 100 mL ultrapure water. The two above described tests were performed, magnetically-stirring the suspensions under UV radiation test.

The two samples were observed by SEM after each of the test at a magnification of x 3000 and x 50 000 (Figure 6).

If the Figure 6 images obtained after UV radiation test are compared to the ones obtained right after preparation (Figure 3). No change can be observed relative to composite powder morphology neither for 1h-IM-AC/TiO_2 nor 10h-IM-AC/TiO_2 sample. Thus, we assumed that the composite sample is stable under its expected use, i.e. under UV radiation. Note that the 10h-IM-AC/TiO_2 sample stability is confirmed under hard mechanical environment, as suggested by the unchanged morphology of this composite powder after sonication. However, note too that after the sonication test, the 1h-IM-AC/TiO_2 powder morphology has changed: AC and TiO_2 can be distinguished separately more easily, suggesting that TiO_2 particles detached from AC surface throughout sonication.

3.2- Multi-functional properties

3.2.1. Adsorption capacity

Adsorption experiments were conducted to track caffeine adsorption over time on each sample. The Langmuir isotherm gave a consistent fit. Langmuir's model assumes a flat and homogeneous surface on which monolayer adsorption occurs [51] and was chosen here as it is in good agreement with the isotherm types of our samples as highlighted previously from N_2 adsorption-desorption experiments. This model is usually described by the equation (2):

$$q_e = \frac{q_{max} b C_e}{1 + b C_e} \quad (2)$$

where q_e is adsorbed quantity at equilibrium ($mg.g^{-1}$), q_{max} is maximum adsorption capacity ($mg.g^{-1}$), b is a constant that is dependent on the energy of adsorption ($L.mg^{-1}$) of the adsorbent/adsorbate pair, and C_e is concentration in liquid phase at equilibrium ($mg.L^{-1}$). All

adsorption isotherms were fitted by the model, then it was used to obtain q_{max} and b values for each sample.

Unmilled AC samples showed the best adsorption capacity, with an asymptotic plateau of saturation at 395 mg/g (Figure 7). The adsorption capacity of IM-AC samples was about 65% of the non-milled samples. These results correlate with BET surface analysis (Table 2), which revealed a loss of total BET surface from 1742 m²/g to 1218 and 1022 m²/g for 1h-IM-AC and 10h-IM-AC, respectively, *i.e.* 60% loss after 1 h and 70% loss after 10 h. The composite IM-AC/TiO_2 conserved its adsorption capacity compared to unmilled AC (90% of the raw AC capacity). Note that caffeine adsorption is reported per gram of carbon in the sample. Previous BET experiments (Table 2) showed no effect of milling on the micropore surface area of AC within composites, so the lower value of micropore surface area in composites compared to unmilled AC is only due to the ratio of TiO_2, which has a very low micropore surface area in the structure.

We can assume that the lower adsorption capacity of IM-AC compared to IM-AC/TiO_2 is conditioned by the occurrence of ball collisions inside the mill involving interactions with AC particles. Grinding AC together with TiO_2 should statistically provide less stress on AC particles compared to milled AC alone. Despite the value of this assumption, it was not verified here as it is beyond the scope of this study. Note that despite their different adsorption capacities, all the samples studied in these experimental conditions had the same type I isotherm (IUPAC), which depicts monolayer adsorption in a mainly microporous network. This observation is consistent with the good fit of experimental curves using the Langmuir model based on the assumption of monolayer adsorption. The Langmuir fitting was performed from experimental data on raw AC, IM-AC and IM-AC/TiO_2 composites (Figure 7). Table 4 reports the computed parameters determined from the model and data of this figure.

The Q_{max} parameter for all samples confirms the conserved adsorption capacity of IM-AC/TiO_2 compared to raw AC and the 35% loss of capacity for AC when it is intermittently milled alone. The b constant characterizes the ability of the adsorbent surface to adsorb the targeted adsorbate. For both IM-AC and unmilled AC, b did not vary, staying at about 0.420–0.450 $L.mg^{-1}$. For IM-AC/TiO_2 composites, b decreased to 0.254 $L.mg^{-1}$, which is obviously due to the presence of TiO_2 which is a very poor adsorbent. These results are in good agreement with the BET analysis (Table 2), which depicted a lower surface area for composite samples and therefore a lower available micropore volume for those materials compared to AC samples.

The maximum amount of adsorbed caffeine on the AC/TiO_2 composite was compared with a recent review [60], which aimed to compare different techniques for caffeine removal from water. A part of this report was dedicated to the comparison of 21 adsorption articles in terms of maximum adsorbed amount (assess by Langmuir model). Six of them refer to adsorption on AC and among them, the highest amount of adsorbed caffeine was of 273 $mg.g^{-1}$. Another review [61] compared the adsorption capacity of 24 different studies, from which the highest amount of caffeine adsorbed on AC was 395 $mg.g^{-1}$. Thus, the comparison of these previous works with our adsorption experiments led us to assert that our AC/TiO_2 composites adsorption capacity is competitive compared to another AC adsorbent.

3.2.2- Photocatalytic degradation experiments

The two steps photodegradation protocol described in section 2.3. enabled us to carry out a photocatalytic activity study separating adsorption phenomena from photocatalytic phenomena. Results were fitted using a simple law of first-order degradation kinetics (3), as the goal was only to compare the apparent kinetic constants to rank the efficiency of the samples:

$$-\frac{dC}{dt} = kC \quad (3)$$

where C is the concentration of caffeine in the liquid ($mg.L^{-1}$), t (s) is time running from 0, which corresponds to UV lamp turned on, and k is the apparent kinetic constant (s^{-1}).

For each composite sample and for unmilled TiO_2, a reference (the same single material or composite studied) was not put under the UV lamp after 180 min in order to highlight the photodegradation provided by the UV lamp. Results are shown in Figure 8.

The adsorption phase can be analyzed to confirm the adsorption properties of TiO_2 and composite samples as discussed with data of Figure 7. First, TiO_2 did not show adsorption properties since as expected, there is no decrease in caffeine concentration for the first 180 min for all TiO_2 samples, *i.e.* raw unmilled TiO_2, 10h-CM-TiO_2 and 10h-IM-TiO_2 (Figure 8). For composite samples, equilibrium reached at 180 minutes corresponds to one point of equilibrium of the isotherm between liquid and solid phase, in the same equilibrium concentration conditions, *i.e.* C_e ~200-210 $mg.L^{-1}$ for both composite samples. In these conditions, adsorbed caffeine quantity on composite isotherms was about 340 $mg.g^{-1}$. Note too that milling time had no influence on relative adsorbed quantity of caffeine on composites, as the equilibrium reached at 180 min showed 90% of the initial caffeine removed from the solution for both composite samples. These observations are in good agreement with the adsorption isotherms that revealed no significant influence of milling time on adsorption properties between 1h-IM-AC/TiO_2 and 10h-IM-AC/TiO_2 composites. As the first period of the experiment is under dark conditions, reference samples obviously expressed the same behavior as the samples under study. For all samples, equilibrium was reached at 180 min, ending with a stabilization of caffeine concentration.

After 180 min, none of the reference samples showed any drop in caffeine concentration, thus highlighting the caffeine concentration stabilized after 180 min when samples were not put under the UV light, which gives us confidence grounds to infer statements concerning the effect of UV radiation on the samples.

Under UV radiation, all samples showed a drop in caffeine concentration except for 10h-CM-TiO_2. The XRD pattern of this sample (Figure 1.C) had revealed a deep phase transformation from anatase to rutile and brookite as well as a significant amorphization, which is responsible for the absence of photocatalytic activity. It appears clear that 10h-IM-TiO_2 is not as good as the raw TiO_2 sample for caffeine removal, but its photocatalytic efficiency is close. XRD pattern of this sample (Figure 1.B) showed that its anatase content was high (79 wt%), giving evidence that the intermittent milling protocol can prevent phase transformation. As a result, this 10h-IM-TiO_2 sample did conserve a great deal of its photocatalytic activity through milling.

The photocatalytic activity of composite samples was lower than for crude TiO_2 and appeared to be quasi-constant through milling time. The slope of the caffeine concentration profile at the initial time points to the apparent rate constant k. 1h-IM-AC/TiO_2 gave a calculated apparent kinetic constant of 1.04×10^{-5} s^{-1}, which is similar to the value given by the 10h-IM-AC/TiO_2 composite (1.00×10^{-5} s^{-1}), thus further showing how milling time has little influence on photocatalytic activity degradation between 1 and 10 h of intermittent milling. The constant calculated for raw TiO_2 was much higher, reaching 12.33×10^{-5} s^{-1}. However, given the aggregate shape of composites observed on SEM images (Figure 3) and BET tests (Table 2), we assume that the lower photodegradation kinetics values for the composites can be attributed to lower available catalyst surface within the composite than for the raw TiO_2 sample, which means that composites have less TiO_2 surface getting irradiated by UV light. This

assumption is confidently supported by the BET results in Table 2 showing that the BET surface of TiO_2 is negligible compared with the value for AC.

To conclude the discussion, it was observed on photo-degradation properties, it was observed in previous reports [62-64], working with different experimental conditions and target molecules, that some AC/TiO_2 composites exhibited photo-oxidation rates as good as pure TiO_2, and sometimes better. Note that all these studies focused on low AC ratio AC/TiO_2 composites. Thus, comparing our photodegradation results with these studies allowed us to suggest the need of further investigation: (i) on the radiative transfer inside composite material suspensions to understand the radiation absorption process inside the particles and (ii) on the change of all functional properties while the composition of AC/TiO_2 powders vary.

4- Conclusions

Here we report, for the first time, that AC/TiO_2 composite materials can be prepared by a one-step mechanosynthesis process. Composites were successfully produced, and their structural properties were controlled through a preliminary characterization effort to gain a further insight on the mechanosynthesis process depending on the selected milling parameters. Continuous milling was found to affect too much the crystallinity and phase composition of the TiO_2 component, and so an intermittent-milling protocol was needed to preserve its structural properties and thus its photocatalytic activity. We characterized the porosity and adsorption capacity of activated carbon through BET analysis and the BJH method. Experiments confirmed partial preservation of porosity, with a loss of 30 to 40% of BET surface area from 1 to 10 h of intermittent milling. Milling time did not profoundly affect the pore size distribution of AC, which kept a monomodal microporous distribution. Morphological and granulometric analysis on composite samples highlighted the need for 10 h of intermittent milling to homogenize both composites particle size and composition. This first part of our work revealed

the necessity for controlled conditions in order to preserve their structural properties and led us to define a set of parameters that preserve the desired properties through mechanosynthesis, i.e. 10 h of milling, interrupted with a 5 min pause every 15 min, and using a rotation speed of 400 rpm.

The second part of this work consisted in evaluating both the adsorption and photocatalytic properties of the as-made intermittently-milled composites. This was achieved through caffeine adsorption and photocatalytic removal experiments. Composite samples preserved their adsorbent properties compared to starting materials, exhibiting a caffeine maximum adsorbed amount of 353 $mg.g^{-1}$, which corresponds to 90% of AC maximum adsorbed amount. The adsorption capacity of the composite samples was affected in the same way whatever the milling time: 1 or 10 h. The photo-oxidation experiments coupled with the assessment of the caffeine apparent photodegradation kinetic constant highlighted that AC/TiO_2 composites exhibit a photocatalytic activity. This constant value was 1.04×10^{-5} s^{-1} and 1.00×10^{-5} s^{-1} respectively for the 1 h and the 10 h intermittently milled AC/TiO_2. It was thus noted that milling time had a negligible effect on both adsorption and photodegradation properties, making the choice of a longer milling time more appropriate because it leads to more homogeneous and controlled composite powders. It was observed that these values were ten times lower than pure TiO_2, and it is assumed to be explained by a lower irradiated catalyst surface within the composite materials.

We thus conclude that mechanosynthesis can successfully synthesize AC/TiO_2 composites for the targeted application, *i.e.* solar water treatment. Further studies are now needed on radiative transfer through the composites in order to better understand the way incident radiation is scattered and absorbed through the suspension. We anticipate that different elaboration parameters, starting materials and/or carbon-to-catalyst ratios should lead to enhanced bifunctional materials for sorption/photodegradation applications.

Please find below the detailed description of the co-authors contribution:

Enrique Ribeiro Investigation, Formal analysis, Visualization, Writing – Original Draft.
Gaël Plantard Conceptualization, Methodology, Supervision.
Vincent Goetz Conceptualization, Methodology, Supervision.
Francis Teyssandier Methodology, Supervision, Validation, Writing – Review & Editing.
Francis Maury Conceptualization, Validation, Writing – Review & Editing.
Denis Chaumont Investigation, Resources.
Najim Sadiki Resources, Formal analysis.

Declaration of interests

The authors declare that they have no known competing financial interests or personal relationships that could have appeared to influence the work reported in this paper.

Acknowledgements

This work was supported by the Occitanie Region in France and by European Regional Development Fund (ERDF) provided by the European Union.

References

[1] Yang Y., Zheng Z., Zhang D., Zhang X, 2020, "Response surface methodology directed adsorption of chlorate and chlorite onto MIEX resin and chemical properties study", Environmental Science: Water Research & Technology. DOI: 10.1039/C9EW01003C

[2] Yang Y., Yang M., Zheng Z., Zhang X., 2020, "Highly effective adsorption removal of perfluorooctanoic acid (PFOA) from aqueous solution using calcined layer-like Mg-Al

hydrotalcites nanosheets", Environmental Science and Pollution Research. DOI: 10.1007/s11356-020-07892-4

[3] Zhang X., Shi X., Chen J., Yang Y., Lu G., 2019, "The preparation of defective UiO-66 metal organic framework using MOF-5 as structural modifier with high sorption capacity for gaseous toluene", Journal of Environmental Chemical Engineering 7 (5), 103405.

[4] Saleh T.A., Tuzen M., Sari A., 2017 "Magnetic activated carbon loaded with tungsten oxide nanoparticles for aluminum removal from waters", Journal of Environmental Chemical Engineering 5 (3), 2853-2860.

[5] Wang Y., Yu L., Wang R., Wang Y., Zhang X., 2020, "Microwave catalytic activities of supported perovskite catalysts $MO_x/LaCo_{0.5}O_3$@CM (M=Mg,Al) for salicylic acid degradation", Journal of Colloid and Interface Science 564, 392-405.

[6] Liu Y., Shen S., Zhang J., Zhong W., Huang X., 2019, "Cu_{2-x}-Se/CdS composite photocatalyst with enhanced visible light photocatalysis activity", Applied Surface Science 478, 762-769.

[7] Malato S., Fernandez-Ibañez P., Maldonado M.I., Blanco J., Gernjak W., 2009, "Decontamination and disinfection of water by solar photocatalysis, recent overview and trends", Catalysis Today 147 (1), 1-59.

[8] Helali S. Polo-Lopez M.I., Fernandez-Ibañez P., Ohtani B., Amano F., Malato S., Guillard C., 2014, "Solar photocatalysis: A green technology for E. Coli contaminated water disinfection. Effect of concentration and different types of suspended catalyst", Journal of Photochemistry and Photobiology A: Chemistry 276, 31-40.

[9] Chong M. N., Jin B., Chow C.W.K., Saint C., 2010, "Recent developments in photocatalytic water treatment technology: A review", Water Research 44 (10), 2997-3027.

[10] Nakata K., Fujishima A., 2012, "TiO_2 photocatalysis: design and applications", Journal of Photochemistry and Photobiology C: Photochemistry Reviews 13 (3), 169-189.

[11] Tsang C.H.A., Li K., Zeng Y., Zhao W., Zhang T., Zhan Y., Xie R., Leung D.Y.C., Huang H., 2019, "Titanium oxide based photocatalytic materials development and their role in the air pollutants degradation: Overview and forecast", Environment International 125, 200-228.

[12] Woan K, Pyrgiotakis G., Sigmund W., 2009, "Photocatalytic carbon-nanotube-TiO_2 composites", Advanced Materials 21 (21), 2233-2239.

[13] Khalid N. R., Majid A., Bilal Tahir M., Niaz N.A., Khalid S., 2017, "Carbonaceous-TiO_2 nanomaterials for photocatalytic degradation of pollutants: A review", Ceramics International 43 (17), 14552-14571.

[14] MiarAlipour S., Friedmann D., Scott J., Amal R., 2018, "TiO_2 porous adsorbents: Recent advances and novel applications", Journal of Hazardous Materials 341, 404-423.

[15] Mahalakshmi M., Vishnu Priya S., Arabindoo B., Palanichamy M., Murugesan V., 2009, "Photocatalytic degradation of aqueous propoxur solution using TiO_2 and Hβ zeolite-supported TiO_2", Journal of Hazardous Materials 161 (1), 336-343.

[16] Plantard G., Correia F., Goetz V., 2011, "Kinetic and efficiency of TiO_2-coated foam or tissue and TiO_2-suspension in a photocatalytic reactor applied to the degradation of the 2,4-dichlorophenol", Journal of Photochemistry and Photobiology A: Chemistry 222 (1), 111-116.

[17] Yu F., Li Y., Han S., Ma J., 2016, "Adsorptive removal of antibiotics from aqueous solution using carbon materials", Chemosphere 153, 365-385.

[18] Foo K.Y., Hameed B.H., 2010, "Detoxification of pesticide waste via activated carbon adsorption process", Journal of Hazardous Materials 175 (1-3), 1-11.

[19] Basaleh A.A., Al-Malack M.H., Saleh T.A., 2019, "Methylene Blue removal using polyamide-vermiculite nanocomposites: Kinetics, equilibrium and thermodynamic study", Journal of Environmental Chemical Engineering 7 (3), 103107

[20] Saleh T.A., Ali I., 2018, "Synthesis of polyamide grafted carbon microspheres for removal of rhodamine B dye and heavy metals", Journal of Environmental Chemical Engineering 6 (4), 5361-5368.

[21] Corwin C.J. Summers R.S., 2011, "Adsorption and desorption of trace organic contaminants from granular activated carbon adsorbers after intermittent loading and throughout backwash cycles", Water Research 45, 417-426.

[22] Saleh T.A., Sari A., Tuzen M., 2017, "Optimization of parameters with experimental design for the adsorption of mercury using polyethylenimine modified-activated carbon", Journal of Environmental Chemical Engineering 5 (1), 1079-1088.

[23] Chen J., Zhang X., Bi F., Zhang X., Yang Y., Wang Y., 2020, "A facile synthesis for uniform tablet-like TiO_2/C derived from Materials of Institute Lavoisier-125(Ti) (MIL-125(Ti)) and their enhanced visible light-driven photodegradation of tetracycline", Journal of Colloid and Interface Science 571, 275-284.

[24] Reddy N.R., Bhargav U., Kumari M.M., Cheralathan K.K., Shankar M.V., Reddy K.R., Saleh T.A., Aminabhavi T.M., 2020, "Highly efficient solar light-driven photocatalytic hydrogen production over Cu/FCNTs-titania quantum dots-based heterostructures", Journal of Environmental Management 254, 109747.

[25] Alves Nunes Simonetti E., Civdanes L.S., Moreira Bastos Campos T., Rossi Canuto de Menezes B., Sales Brito F., Patrocinio T., 2016, "Carbon and TiO_2 synergistic effect on methylene blue adsorption", Materials Chemistry & Physics 177, 330-338.

[26] Li Puma G., Bono A., Krishnaiah D., Collin J.G., 2008, "Preparation of titanium dioxide photocatalyst loaded onto activated carbon support using chemical vapor deposition: A review paper", Journal of Hazardous Materials 157 (2-3), 209-219.

[27] Telegang Chekem C., Richardson Y., Plantard G., Blin J., Goetz V., 2016, "From biomass residues to titania coated carbonaceous photocatalysts: A comparative analysis of different preparation routes for water treatment application", Waste & Biomass Valorization 8 (8), 2721-2733.

[28] Goetz V., Janin T., Plantard G., Brosillon S., 2013, "Hybridation between heterogenous photocatalysis and adsorption", International Journal of Engineering Practical Research 2 (3), 86-93.

[29] Pow-Seng Y. Teik-Thye L., 2012, "Solar regeneration of powdered activated carbon impregnated with visible-light responsive photocatalyst: Factors affecting performances and predictive model", Water Research 46 (9), 3054-3064.

[30] TelegangChekem C., Goetz V., Richardson Y., Plantard G., Blin J., 2019, "Modeling of adsorption/photodegradation phenomena on AC-TiO_2 composite catalysts for water treatment detoxification", Catalysis Today 328, 183-188.

[31] Leary R., Westwood A., 2011, "Carbonaceous nanomaterials for the enhancement of TiO_2 photocatalysis", Carbon 49 (3), 741-772.

[32] Gu Y., Yperman J., Carleer R., D'Haen J., Maggen J., Vanderheyden S., Vanreppelen K., Machado Garcia R., 2019, "Adsorption and photocatalytic removal of Ibuprofen by activated carbon impregnated with TiO_2 by UV-Vis monitoring", Chemosphere 217, 724-731.

[33] Ouzzine M., Romero-Anaya A.J., Lillo-Rodenas M.A., Linares-Solano A., 2014, "Spherical activated carbon as an enhanced support for TiO_2/AC photocatalysts", Carbon 67, 104-118.

[34] Azizi F., 2017, "Synthesis and characterization of grapheme-N-doped TiO_2 nanocomposites by sol-gel method and investigation of photocatalytic activity", Journal of Materials Science: Materials in Electronics 28 (15), 11222-11229.

[35] Koli V.B., Dhodamani A.G., Delekar S.D., Pawar S.H., 2017, "In situ sol-gel synthesis of anatase TiO_2-MWCNTs nanocomposites and their photocatalytic applications", Journal of Photochemistry and Photobiology A: Chemistry 333, 40-48.

[36] Zhang X., Zhou M., Lei L., 2006, "TiO_2 Photocatalyst deposition by MOCVD on activated carbon", Carbon 44 (2), 325-333.

[37] Ma L., Chen A., Zhang Z., Lu J., He H., Li C., 2012, "In-situ fabrication of CNT/TiO_2 interpenetrating network film on nickel substrate by chemical vapor deposition and application in photoassisted water electrolysis", Catalysis Communications 21, 27-31.

[38] Awfa D., Ateia M., Fujii M., Johnson M.S., Yoshimura C., 2018, "Photodegradation of pharmaceuticals and personal care products in water treatment using carbonaceous-TiO_2 composites: A critical review of recent literature", Water Research 142, 26-45.

[39] James S.L., Adams C.J., Bolm C., Braga D., Collier P., Friscic T., Grepioni F., Harris K.D.M., Hyett G., Jones W., Krebs A., Mack J., Maini L., Orpen A.G., Parkin I.P., Shearous W.C., Steed J.W., Waddell D.C., 2012, "Mechanochemistry : opportunities for new and cleaner synthesis", Chemical Society Reviews 41, 413-447.

[40] Tanaka K., Toda F., 2000, "Solvent-Free Organic Synthesis", Chemical Reviews 100 (3), 1025-1074.

[41] Kaupp G., 2009, "Mechanochemistry: the varied applications of mechanical bond-breaking", CrystEngComm 11 (3), 388-403.

[42] Kaupp G., 2011, "Reactive milling with metals for environmentally benign sustainable production", CrystEngComm. 13 (9), 3108.

[43] Wang G-W, 2013, "Mechanochemical organic synthesis", Chemical Society Reviews 42 (18), 7668-7700.

[44] Choulier D., Rahoudj R., Gaffet E., 1997, "Mechanics of mechanosynthesis: State of the art and prospective", Annales de Chimie Science des Materiaux 22, 351-361.

[45] Suryanarayana C., 2001, "Mechanical alloying and milling", Progress in Materials Science 46, 1-184.

[46] Cunha C.A., Correa O.V., Sayeg I.J., Lima N.B., Ramanathan L.V., 2016, "Structural and thermodynamic properties of nanocrystalline Cr_3C_2-25(Ni_2OCr) composite powders produced by high-energy ball milling", Journal of Thermal Analysis and Calorimetry 126 (3), 1447-1453.

[47] Davis R.M., Koch C.C., 1986, "Mechanical alloying of brittle components: Silicon and Germanium", Scripta Metallurgica 21 (3), 305-310.

[48] Miao J., Zhang R., Zhang L., 2018, "Photocatalytic degradations of three dyes with different chemical structures using ball-milled TiO_2", Materials Research Bulletin 97, 109-114.

[49] Palma D., Prevot A.B., Brigante M., Fabbri D., Magnacca G., Richard C., Mailhot G., Nistico R., 2018, "New insights on the Photodegradation of Caffeine in the Presence of Bio-Based Substances-Magnetic Iron Oxide Hybrid Nanomaterials", Materials 11 (7), 1084.

[50] Plantard G., Janin T., Goetz V., Brosillon S., 2012, "Solar photocatalysis treatment of phytosanitary refuses: Efficiency of industrial photocatalysts", Applied Catalysis B: Environmental 115-116, 38-44.

[51] Miguet M., Goetz V., Plantard G., Jaeger Y., 2015, "Removal of a chlorinated volatile organic compound (perchloroethylene) from aqueous phase by adsorption on activated carbon", Ind. Eng. Chem. Res. 54 (40), 9813-9823.

[52] Yuangpho N., Le. S.T.T., Treerujiraphapong T., Khanitchaidecha W., Nakaruk A., 2015, "Enhanced photocatalytic performance of TiO_2 particles via effect of anatase-rutile ratio", Physica E: Low-dimensional Systems and Nanostructures 67, 18-22.

[53] Rietveld H.M., 1969, "A profile refinement method for nuclear and magnetic structures", Journal of Applied Crystallography 2 (2), 65-71.

[54] Rezaee M., Khoie S., Liu H.K., 2011, "The role of brookite in mechanical activation of anatase-to-rutile transformation of nanocrystalline TiO_2: An XRD and Raman spectroscopy investigation", Cryst. Eng. Comm. 13 (16), 5055-5061.

[55] Li S., Jiang Z.H., Jiang Q., 2008, "Thermodynamic phase stability of three nano-oxides", Materials Research Bulletin 43, 3149-3154.

[56] H. Zhang, J. Banfield, 1998, "Thermodynamic analysis of phase stability of nanocrystalline titania," Journal of Materials Chemistry 8(9), 2073.

[57] H. Zhang, J. Banfield, 2000, "Understanding polymorphic phase transformation behavior during growth of nanocrystalline aggregates: insights from TiO_2," Journal of Physical Chemistry B 104, 3481.

[58] IUPAC, 1994, "Recommendations for the characterization of porous solids", Pure & Applied Chemistry 66 (8), 1739-1758.

[59] K.S.W. Sing, Everett D.H., Haul R.A.W., Moscou L., Pierotti R.A., Rouquerol J., Siemieniewska T., 1985, "Reporting physisorption data for gas/solid systems with special reference to the determination of surface area and porosity", Pure & Applied Chemistry 57 (4), 603-619.

[60] Rigueto C.V.T., Nazari M.T., De Souza C.F., Cadore J.S., Brião V.B., Piccin J.S., 2020, "Alternative techniques for caffeine removal from wastewater: An overview of opportunities and challenges", Journal of Water Process Engineering 35, 101231.

[61] Anastopoulos I., Pashalidis I., Orfanos A.G., Manariotis I.D., Tatarchuk T., Sellaoui L., Bonilla-Petriciolet A., Mittal A., Nuñez-Delgado A., 2020, "Removal of caffeine, nicotine and amoxicillin from (waste)waters by various adsorbents. A review", Journal of Environmental Management 261, 110236.

[62] Matos J., Miralles-Cuevas S., Ruiz-Delgado A., Oller I., Malato S., 2017, "Development of TiO_2-C photocatalysts for solar treatment of polluted water", Carbon 122, 361-373.

[63] Torimoto T., Okawa Y., Takeda N., Yoneyama H., 1997, "Effect of activated carbon content in TiO_2-loaded activated carbon on photodegradation behaviors of dichloromethane", Journal of Photochemistry and Photobiology A: Chemistry 103, 153-157.

[64] Liu S.X., Chen X.Y., Chen X., 2007, "A TiO_2/AC composite photocatalyst with high activity and easy separation prepared by a hydrothermal method", Journal of Hazardous Materials 143, 257-263.

Figure captions

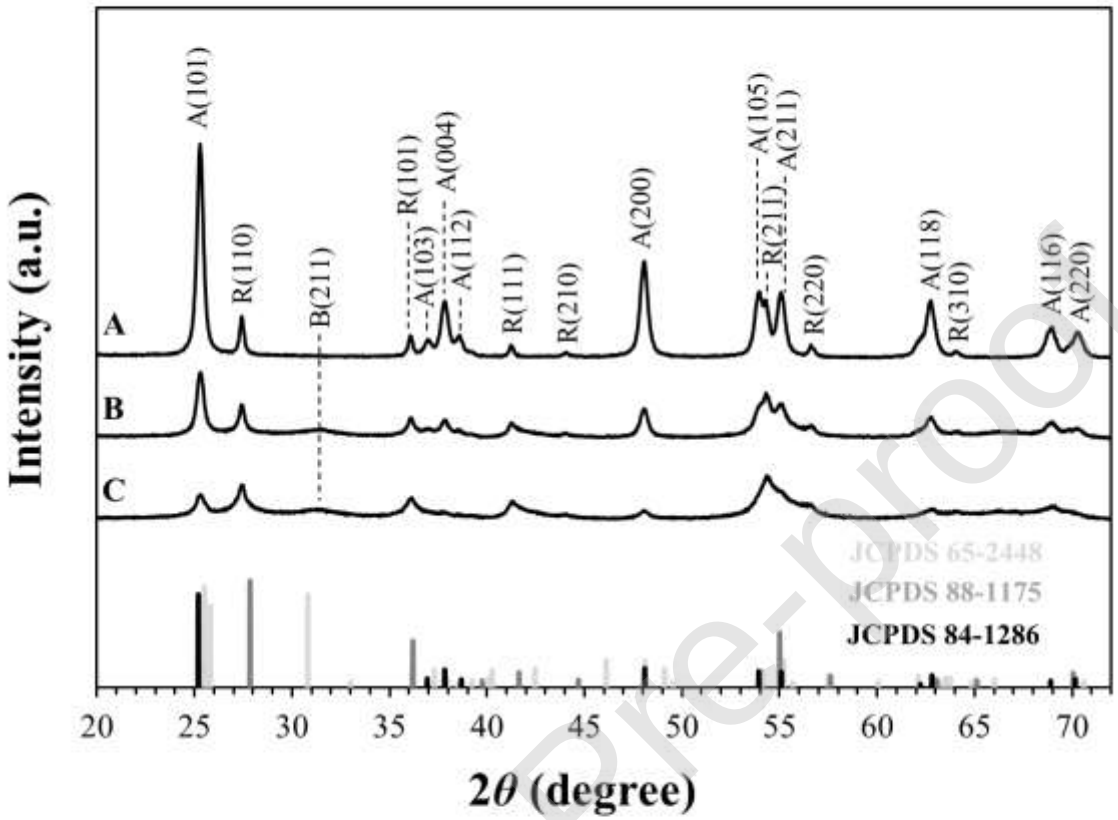

Figure 1. XRD pattern of the raw unmilled TiO_2 (sample a) compared with 10h-IM-TiO_2 (sample b) and 10h-CM-TiO_2 (sample c). Anatase (A), Rutile (R) and Brookite crystal planes are indexed as well as their matching JCPDS data files: respectively JCPDS n°84-1286; 88-1175; 65-2448.

Figure 1. XRD pattern of the raw unmilled TiO_2 (sample a) compared with 10h-IM-TiO_2 (sample b) and 10h-CM-TiO_2 (sample c). Anatase (A), Rutile (R) and Brookite crystal planes are indexed as well as their matching JCPDS data files: respectively JCPDS n° 84-1286; 88-1175; 65-2448.

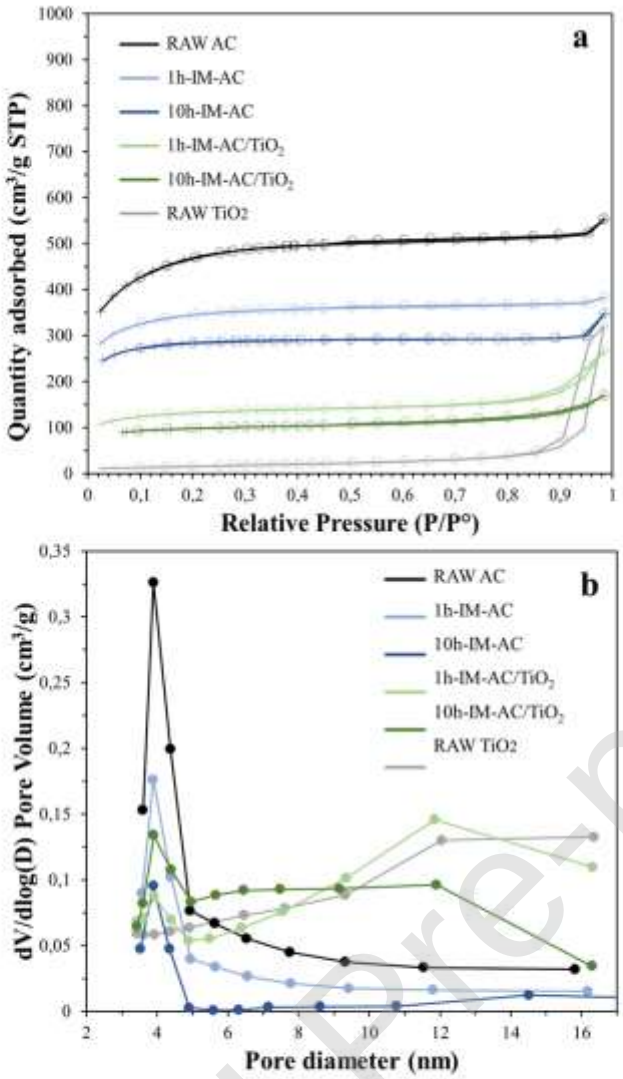

Figure 2. N_2 adsorption(+)/desorption(o) isotherms (a) and corresponding pore-size distribution curves (b) of raw materials (AC and TiO_2) and intermittently milled (AC, TiO_2, and composites) samples.

Figure 2. N_2 adsorption(+)/desorption(o) isotherms (a) and corresponding BJH pore-size distribution curves (b) of raw materials (AC and TiO_2) and intermittently milled (AC, TiO_2, and composites) samples.

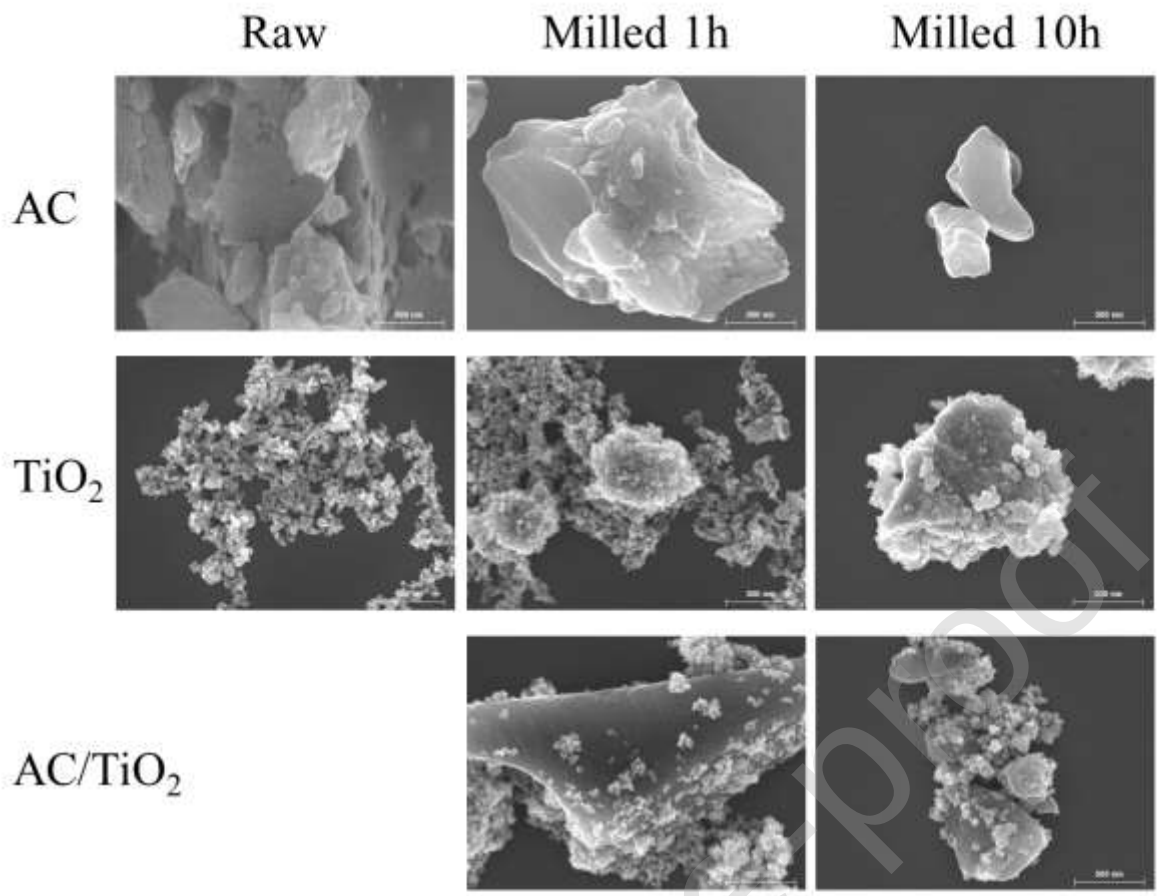

Figure 3. Scanning electron images (SEM-FEG, Hitachi S-4500) of raw and milled samples. Images recorded with a secondary electron detector at 5 kV electron beam for a working distance of 5 mm and a x 50 000 magnification. Left to right: increasing milling time as shown on top. Top to bottom: milled material as shown on the left (AC; TiO_2; AC/TiO_2 composites).

Figure 3. Scanning electron images (SEM-FEG, Hitachi S-4500) of raw and milled samples. Images recorded with a secondary electron detector at 5 kV electron beam for a working distance of 5 mm and a x 50 000 magnification. Left to right: increasing milling time as shown on top. Top to bottom: milled material as shown on the left (AC; TiO_2; AC/TiO_2 composites).

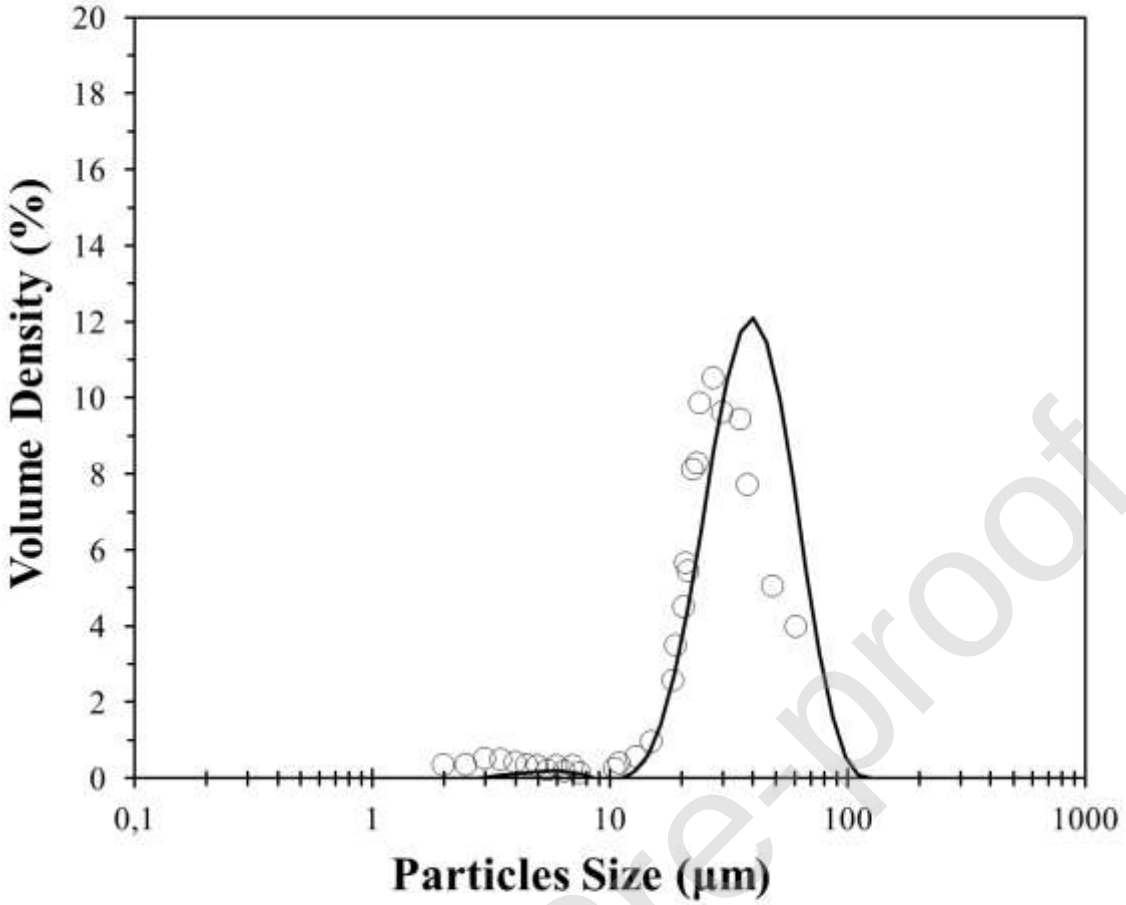

Figure 4. Particles size distribution of Raw TiO_2. Cross-check between DLS (-) and Image treatment (o) methods.

Figure 4. Particles size distribution of Raw TiO_2. Cross-check between DLS using Mie theory (-) and statistical image treatment of 10 000 particles (o) methods.

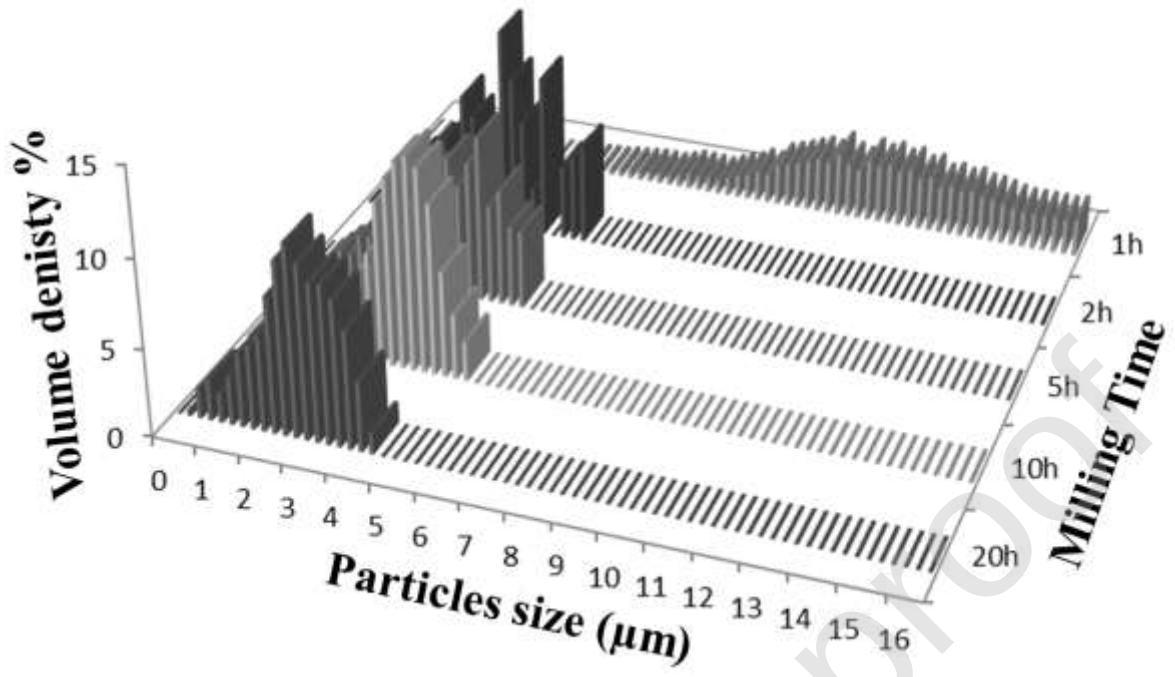

Figure 5. Image treatment method results of granulometric analysis of composites powders intermittently milled for different times: 1h (A) ; 2h (B) ; 5h (C) ; 10h (D) ; 20h (E).

Figure 5. Image treatment method results of granulometric analysis of AC/TiO_2 composites powders intermittently milled for different times: 1h (A) ; 2h (B) ; 5h (C) ; 10h (D) ; 20h (E).

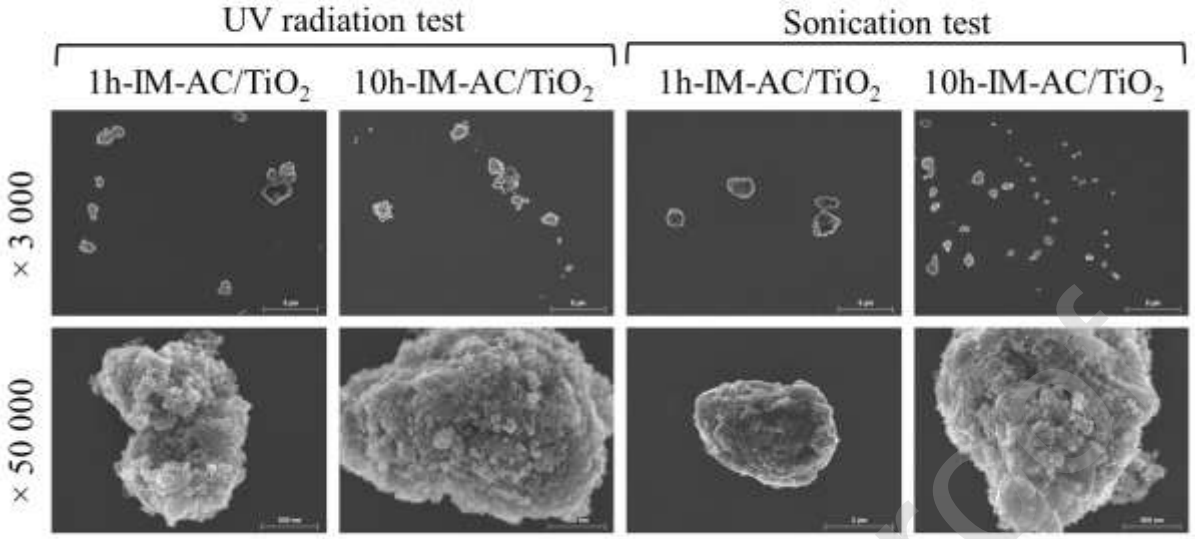

Fig. 6. Scanning electron images (SEM-FEG, Hitachi S-4500) of 1h-IM-AC/TiO_2 and 10h-IM-AC/TiO_2 samples after UV-radiation test and after sonication test. Images recorded with a secondary electron detector at 5 KV electron beam for a working distance of 5 mm. Top to bottom : magnification values, as shown on the left.

Fig. 6. Scanning electron images (SEM-FEG, Hitachi S-4500) of 1h-IM-AC/TiO_2 and 10h-IM-AC/TiO_2 samples after UV-radiation test and after sonication test. Images recorded with a secondary electron detector at 5 KV electron beam for a working distance of 5 mm. Top to bottom: magnification values, as shown on the left.

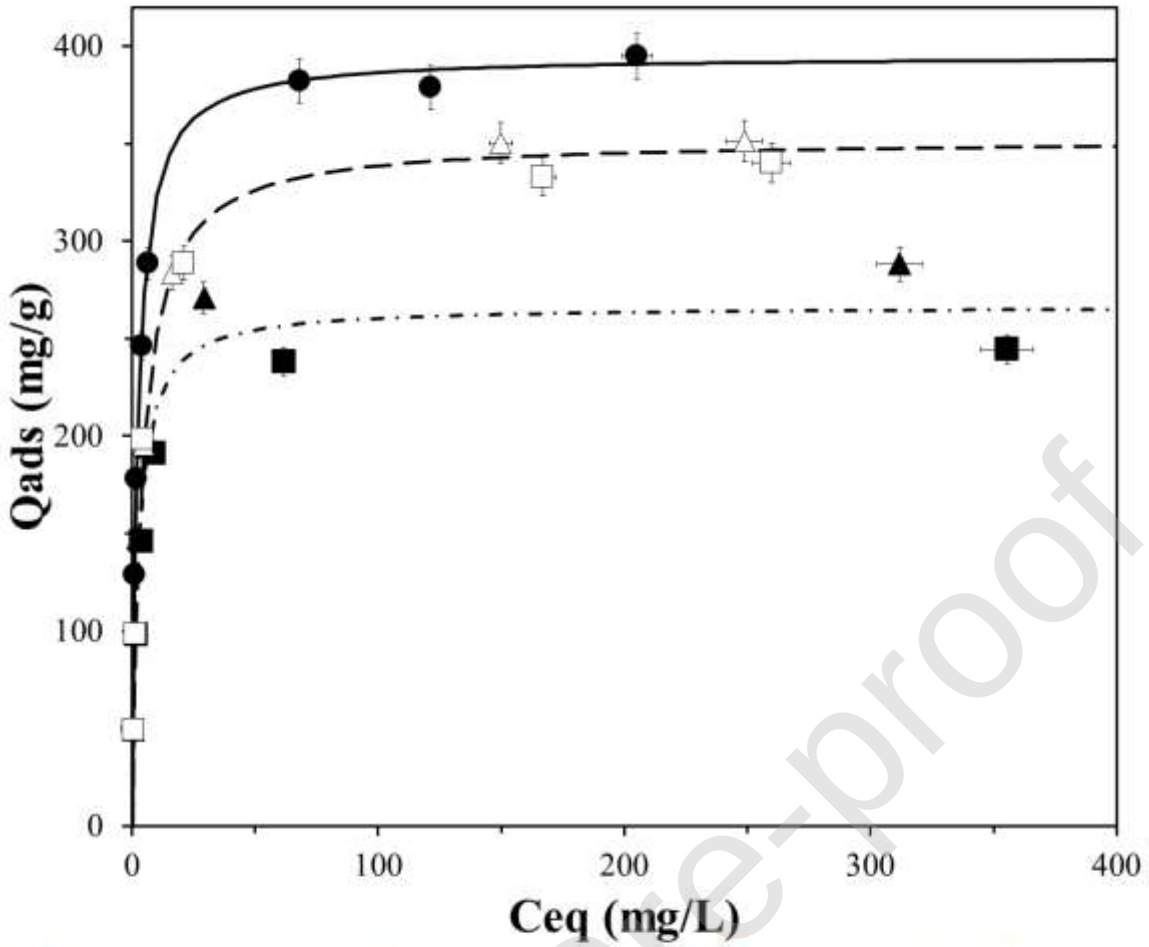

Figure 7. Adsorption isotherms for caffeine onto raw Activated Carbon (●) intermittently milled at different time: 1h-IM-AC (▲) ; 10h-IM-AC (■). Comparison with Composites Activated Carbon/TiO_2 prepared by mechanosynthesis using the intermittent protocol: 1h-IM-AC/TiO2 (△) ; 10h-IM-AC/TiO2 (□). The continuous and dash lines correspond to the fitted Langmuir model.

Figure 7. Adsorption isotherms for caffeine onto raw Activated Carbon (●) intermittently milled at different time: 1h-IM-AC (▲) ; 10h-IM-AC (■). Comparison with Composites Activated Carbon/TiO_2 prepared by mechanosynthesis using the intermittent protocol: 1h-IM-AC/TiO2 (△) ; 10h-IM-AC/TiO2 (□). The continuous and dash lines correspond to the fitted Langmuir model.

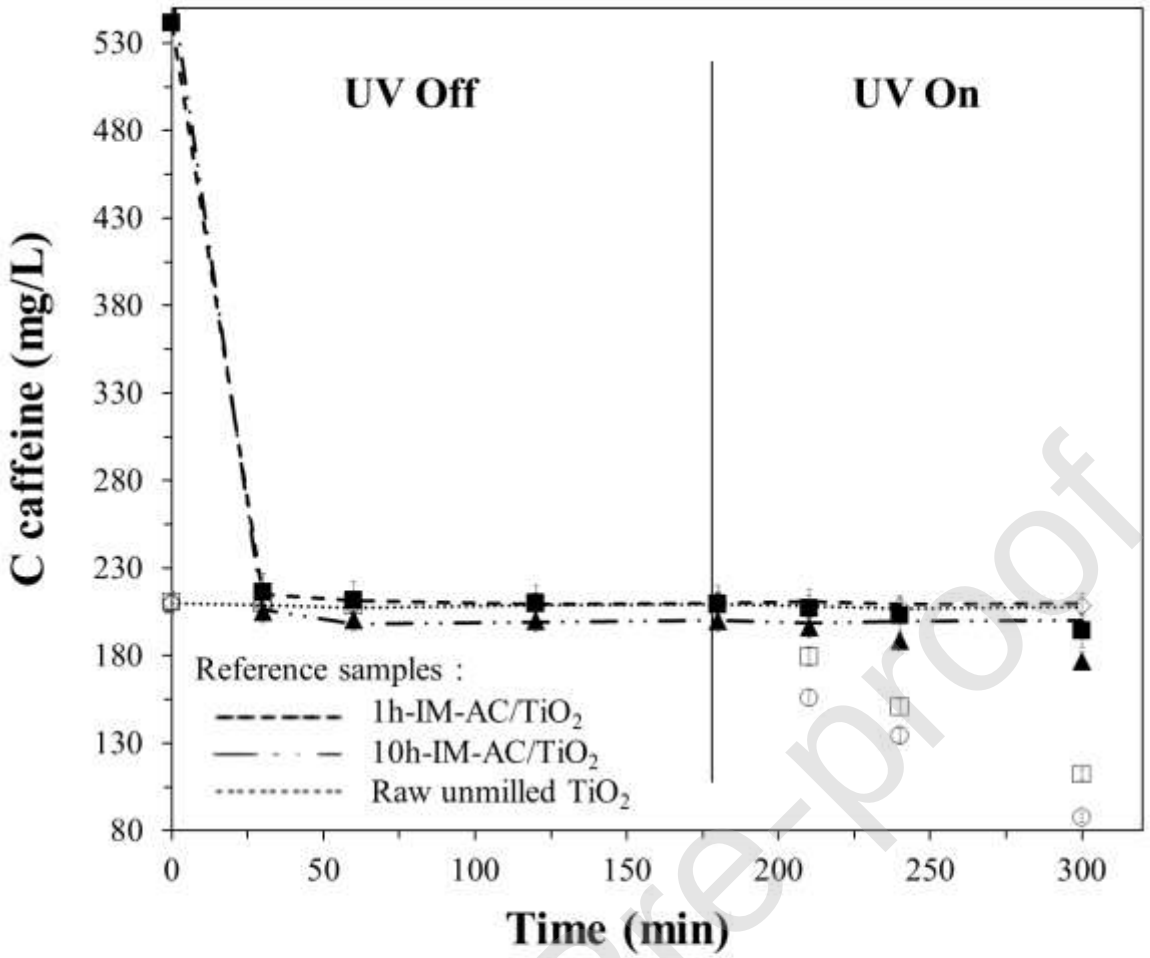

Figure 8. Caffeine adsorption followed by photocatalytic degradation experiments on TiO_2: unmilled TiO_2 (O), 10h-CM-TiO_2 (◊) and 10h-IM-TiO_2 (□). Comparison with the composite materials 1h-IM-AC/TiO_2 (▲) and 10h-IM-AC/TiO_2 (■). Reference samples are reported with lines.

Figure 8. Caffeine adsorption followed by photocatalytic degradation experiments on TiO2: unmilled TiO2 (O), 10h-CM-TiO2 (◊) and 10h-IM-TiO2 (□). Comparison with the composite materials 1h-IM-AC/TiO2 (▲) and 10h-IM-AC/TiO2 (■). Reference samples are reported with lines.

Table legends

Table 1. Phases composition and crystallite diameter calculated respectively via Rietveld method and Scherrer formula for raw TiO_2 (A) and milled one Intermittently (B) or Continuously (C) for 10 h (respectively 10h-IM-TiO_2 and 10h-CM-TiO_2).

Crystallographic Arrangement	**Parameters**	**RAW TiO2 (A)**	**10h Alternately milled TiO2 (B)**	**10h Continuously milled TiO2 (C)**
Anatase	Crystallite diameter (nm)	26	16	9
	Weight percentage	84.9	79	15.6
Rutile	Crystallite diameter (nm)	23	15	9
	Weight percentage	15.1	21	45
Brookite	Crystallite diameter (nm)	-	-	-
	Weight percentage	0	0	39.4

Table 2. BET surface analysis and BJH mean pore volume results for raw materials (AC and TiO_2) and intermittently milled (AC, TiO_2 and AC/TiO_2 composites) samples.

Sample	S_{BET} (m^2/g)	External surface area (m^2/g)	Micropore area (m^2/g)	BJH desorption average pore diameter (nm)
RAW TiO2	57	29	28	8.34
RAW AC	1742	975	767	-
1h-IM-AC	1218	556	662	-
10h-IM-AC	1 022	403	619	-
1h-IM-AC/TiO_2	442	212	230	-
10h-IM-AC/TiO_2	342	121	221	-

Table 3. EDS analysis: mean values of composition after 10 analysis made on each composite sample (intermittently milled for 1 h and 10 h) and calculated standard deviation.

Samples	**C**		**O**		**Ti**	
	wt. %	**Std. Deviation %**	**wt. %**	**Std. Deviation %**	**wt. %**	**Std. Deviation %**
1h-IM-AC/TiO_2	25.8	5.6	30.8	6.2	43.4	5.1
10h-IM-AC/TiO_2	29.5	3.9	29.4	4.1	41.1	3.3

Table 4. Langmuir parameters extracted from experimental fitting of raw AC, intermittently milled AC and intermittently milled AC/TiO_2 composites samples.

Langmuir model parameters $q_e = \frac{q_{max} b C_e}{1 + b C_e}$		**RAW AC**	**Milled AC**	**Milled AC/TiO2**
	b (L.mg^{-1})	0.450	0.420	0.254
	Qmax (mg.g$^{-1}_{of\ carbon}$)	395.0	266.5	353.0
	R^2	0.978	0.958	0.963